Eur. Phys. J. D **39**, 307–312 (2006)
DOI: 10.1140/epjd/e2006-00099-9

THE EUROPEAN PHYSICAL JOURNAL D

Optimization and limits of optical nonlinear measurements using imaging technique

J.-L. Godet[a], H. Derbal, S. Cherukulappurath, and G. Boudebs

Laboratoire des Propriétés Optiques des Matériaux et Applications, UMR CNRS 6136, Université d'Angers, 2 boulevard Lavoisier, 49045 Angers, France

Received 23 February 2006 / Received in final form 20 March 2006
Published online 5 May 2006 –

Abstract. We report on analytical calculations for a $4f$ coherent imaging system in presence of a phase object at the entry of the set-up. We give the results of the optimized parameters to be used in this system so as to increase the sensitivity of the measurement of the nonlinear refraction coefficient. Analytical and previously reported simulated image profiles are compared here. Our study also gives the limits of the nonlinear imaging technique with a phase object for relatively high nonlinear phase shifts.

PACS. 42.65.-k Nonlinear optics – 42.30.Kq Fourier optics

1 Introduction

Recently a *nonlinear-imaging technique with phase-object* (NIT-PO) at the entry of a $4f$ coherent imaging system to characterize the value of the nonlinear refractive index (n_2) of materials placed in the Fourier plane of the set-up [1] was reported. The Fraunhofer diffracted image intensity profile was studied at the output plane (CCD camera) of the optical system. The self-diffracted spectrum on the spatial filter (phase and/or amplitude created by the incident spectrum intensity into the nonlinear material) gives rise to changes into the transmitted intensity at the image plane. The experimental acquisitions were fitted by a simple theoretical model based on Fourier optics to obtain the nonlinear coefficient. In this method, the optical alignment is easy and no scanning of the sample is needed unlike in Z-scan method [2]. Moreover, this technique allows shot-by-shot measurements of n_2 and thus the kinetics of photo-induced effects can be studied [3]. Furthermore, it is possible to characterize n_2 in presence of nonlinear absorption and to obtain a signal that is approximately due to pure nonlinear dephasing using two intense laser shot in the material [4]. This can be done by subtracting the images obtained with and without the phase object (PO), both taken in the nonlinear regime. However, as no analytical solution was readily available, up to now, to characterize the field amplitude in the Fourier plane when a phase object is centered at the entry of the system, the beam was propagated from the object plane to the image plane using the Fresnel diffraction integrals [4].

[a] e-mail: jean-luc.godet@univ-angers.fr

In this paper we develop an analytical solution for the field at the focus of a $4f$ system, at first for a better comprehension of the physical phenomenon. In the case of high numerical aperture lenses, and a relatively large object compared to the spatial resolution, the optical transfer function (OTF) can be neglected [5]. Consequently, in order to simplify the analysis and the calculations we consider an infinite pupil function describing the optical system. We show, both analytically and numerically, that the signal obtained at the exit of the set-up is approximately linear with respect to the induced nonlinear phase, as long as the value of this phase is lower than 1 radian. We provide a simple, linear expression relating the signal to the induced nonlinear phase shift. This allows an easy experimental determination of n_2 at low incident intensities. We also give the optimized parameters for such a system in order to increase the sensitivity of the measurement.

Finally, we consider high values of the nonlinear dephasing induced in the nonlinear material. At high intensities, needed to produce highly nonlinear phase shifts, other nonlinear phenomena could be induced in the sample. In what follows, nonlinear effects of order higher than three are neglected and stimulated scatterings (Brillouin, Raman, and Rayleigh) are not taken into account. It is assumed that the power remains under the self-focusing threshold. Moreover, thermo-optical effects are not significant when one is using ultrashort pulses in the picosecond range. Admittedly, it is not always possible to visualize the phase contrast effect independently from the aforementioned phenomena. However, the theoretical knowledge of the evolution of the phase contrast makes possible, in a first step, to approach the final behavior of the sample

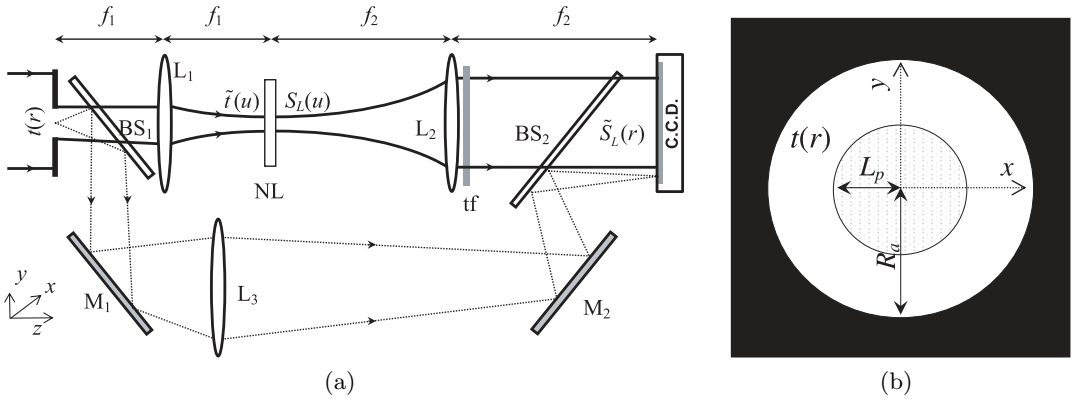

Fig. 1. (a) Schematic of a $4f$ coherent system imager using a phase object (PO). The nonlinear material (NL) is placed in the Fourier plane between lenses L_1 and L_2. A neutral filter (tf) is located after L_2. Intensities are measured relative to a reference signal obtained by using beam splitters BS_1 and BS_2, mirrors M_1 and M_2 and lens L_3. (b) Schematic of the phase object (PO) used at the entry of the set-up.

under study. In particular for high nonlinear dephasing, we will show that a positive contrast (negative contrast) is not always induced by a positive n_2 (negative n_2).

2 Analytical calculations

It is assumed that Fourier optics is sufficient to describe image formation using a $4f$ system [5]) as shown in Figure 1a. At the entrance of the set-up a circular phase object of radius L_p, characterized by a uniform phase shift φ_L, is centered inside an aperture of radius R_a where $R_a > L_p$ (see Fig. 1b). A nonlinear sample considered as 'thin' is located at the focal plane of lens L_1.

2.1 Field amplitude in the focal plane of lens L_1

Let us consider an incident unit-amplitude linearly polarized monochromatic plane wave at normal incidence at the entry of the object. The amplitude transmittance function t, characterizing the object, can be expressed with respect to the radial coordinate r:

$$t(r) = \mathrm{circ}(r/R_a) + [\exp(j\varphi_L) - 1]\mathrm{circ}(r/L_p), \quad (1)$$

where $\mathrm{circ}(x)$ stands for the circ function ($\mathrm{circ}(x) = 1$ if $x < 1$ and $\mathrm{circ}(x) = 0$ otherwise). The field amplitude in focal plane is proportional to $\tilde{t}$, the spatial Fourier transform of t. A simple analytical calculation using the Bessel generating function shows that (see e.g. Ref. [5]):

$$\tilde{t}(u) = \pi R_a^2 \left(\frac{2J_1(2\pi u R_a)}{2\pi u R_a} + \rho^2[\exp(j\varphi_L) - 1]\frac{2J_1(2\pi u \rho R_a)}{2\pi u \rho R_a} \right), \quad (2)$$

where $u = r/(\lambda f_1)$ is the radial spatial frequency with f_1 denoting the focal length of L_1 and $\rho = L_p/R_a$ is a geometrical factor characterizing the object. The intensity $\tilde{I}(u)$ of the laser beam in the focal plane at the entry of the nonlinear sample is proportional to $\zeta(2\pi u R_a) = \tilde{t}(u)\tilde{t}(u)^*/(\pi^2 R_a^4)$, where:

$$\zeta(v) = \left(\frac{2J_1(v)}{v}\right)^2 - 4\rho^2 \left(\frac{2J_1(v)}{v} - \frac{2J_1(v\rho)}{v\rho}\rho^2\right) \times \frac{2J_1(v\rho)}{v\rho}\sin^2\frac{\varphi_L}{2}. \quad (3)$$

Moreover without any phase object ($\rho = 0$), the peak-intensity at the center of the beam is equal to I_0. Therefore, $\tilde{I}(u) = I_0\zeta(2\pi u R_a)$.

The nonlinear sample placed at the Fourier plane is characterized by: α, the linear absorption; β, the nonlinear absorption; n_2, the nonlinear index coefficient. According to reference [6], the nonlinear phase shift at the exit face of this "thin" sample is given by

$$\varphi_{NL}(u) = \frac{kn_2}{\beta}\ln\left(1 + \beta L_{eff}\tilde{I}(u)\right), \quad (4)$$

where $k = 2\pi/\lambda$ is the modulus of the wave vector, and $L_{eff} = (1 - \exp(-\alpha L))/\alpha$ (L denoting the thickness of the material). We define $\varphi_0 = kn_2 L_{eff} I_0$ as the nonlinear phase shift at the center of the beam ($r = 0$) and without PO ($\rho = 0$). By introducing a dimensionless parameter $q_0 = \beta L_{eff} I_0$, we obtain:

$$\varphi_{NL}(u) = \varphi_0 \mathrm{Z}(2\pi u R_a), \quad (5)$$

where:

$$\mathrm{Z}(v) = \frac{\ln(1 + q_0\zeta(v))}{q_0}. \quad (6)$$

For small values of q_0, $\mathrm{Z}(v) \approx \zeta(v)$ because $\zeta(v)$ is a bounded function.

As it can be derived from reference [6], the complex distribution of the field amplitude at the output of the specimen is proportional to:

$$S_L(u) = \tilde{t}(u)\frac{e^{-\alpha L/2}}{\sqrt{1 + q_0}}e^{j\varphi_{NL}(u)}. \quad (7)$$

2.2 Intensity in the image plane

In the image plane $\tilde{S}_L(r)$, the field amplitude after the second lens L_2 (see Fig. 1a), is given by another Fourier transform. Using the property of Bessel functions $y\int_0^\infty J_0(x)J_1(xy)dx = \mathrm{circ}\,(1/|y|)$, we get:

$$\tilde{S}_L(r) = \frac{e^{-\alpha L/2}}{\sqrt{1+q_0}}\left\{\mathrm{circ}(r/R_a) + a_0^{(\rho)}(r) + \left(e^{j\varphi_L}-1\right)\left(\mathrm{circ}(r/L_p) + a_1^{(\rho)}\right)\right\}, \quad (8)$$

where the functions $a_i^{(\rho)}(r)$ ($i = 0$ or 1) are defined by:

$$a_i^{(\rho)}(r) = \int_0^\infty \left[\exp\left(j\varphi_0 \mathrm{Z}(v/b_i,\rho,\varphi_L)\right) - 1\right] \times J_0\left(vr/(R_a b_i)\right) J_1(v)\, dv, \quad (9)$$

with $b_0 = 1$ and $b_1 = \rho$. Moreover, equation (8) may be written in a more compact form:

$$\tilde{S}_L(r) = \frac{e^{-\alpha L/2}}{\sqrt{1+q_0}}\left\{t(r) + a_0^{(\rho)}(r) + \left(e^{j\varphi_L}-1\right)a_1^{(\rho)}(r)\right\}. \quad (10)$$

The complex integrals $a_i^{(\rho)}(r)$ can be decomposed into two real integrals, $c_i^{(\rho)}(r)$ and $s_i^{(\rho)}(r)$, with $a_i^{(\rho)}(r) = c_i^{(\rho)}(r) + j s_i^{(\rho)}(r)$. Calculations of these r-dependent integrals (hereafter simply designated as c_i and s_i respectively) are direct and the intensities $I(r) = \tilde{S}_L(r)\tilde{S}_L(r)^*$ in the image plane can be numerically evaluated for any values of r, ρ, φ_0 and φ_L. Defining a 'normalized' intensity $I^{(\rho)}(r)$ as the ratio $I(r)\sqrt{1+q_0}/[I_0\exp(-\alpha L)]$, we obtain:

$$\begin{aligned} I^{(\rho)}(r) = {} & \mathrm{circ}(r/R_a)\left[1 + 2c_0 - 2\left(2c_1\sin^2\frac{\varphi_L}{2} + s_1\sin\varphi_L\right)\right] \\ & + \mathrm{circ}(r/L_p)\left[2s_0\sin\varphi_L - 4\left(c_0 - 2c_1\right)\sin^2\frac{\varphi_L}{2}\right] \\ & + c_0^2 + s_0^2 + 4\left(c_1^2 + s_1^2 - c_1c_0 - s_1s_0\right)\sin^2\frac{\varphi_L}{2} \\ & - 2\left(c_0s_1 - s_0c_1\right)\sin\varphi_L. \end{aligned} \quad (11)$$

Particularly for $\varphi_L = \pi/2$, equation (11) reduces to:

$$\begin{aligned} I^{(\rho)}(r) = {} & \mathrm{circ}(r/R_a)\left(1 + 2c_0 - 2c_1 - 2s_1\right) \\ & + 2\mathrm{circ}(r/L_p)\left[s_0 - c_0 + 2c_1\right] \\ & + c_0^2 + s_0^2 + 2\left[c_1\left(c_1 - c_0 + s_0\right)\right. \\ & \left. + s_1\left(s_1 - s_0 - c_0\right)\right]. \end{aligned} \quad (12)$$

3 Results and discussion

In Figure 2, we present a comparison between the numerically simulated normalized intensity given in reference [1] and the intensity obtained here from equation (12) for $\rho = L_p/R_a = 0.345$ and $\varphi_0 = 0.91$ rad. A comparison

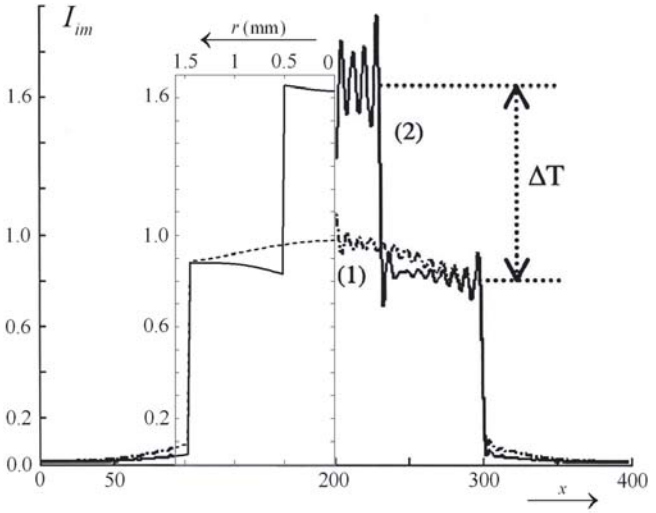

Fig. 2. Comparison of numerical simulations reported in reference [1] (right side of the profile) and analytical calculations (left side). Profile (1): top-hat beam image at the output of the $4f$ set-up after transmission through a lossless Kerr material inducing a nonlinear phase shift $\varphi_0 = 0.91$ rad (dashed line); profile (2): top-hat beam image when a PO is centered at the entry of the set-up (solid line). In this figure, the phase of the PO is $\varphi_L = \pi/2$ and its geometrical parameter is $L_p/R_a = 0.345$.

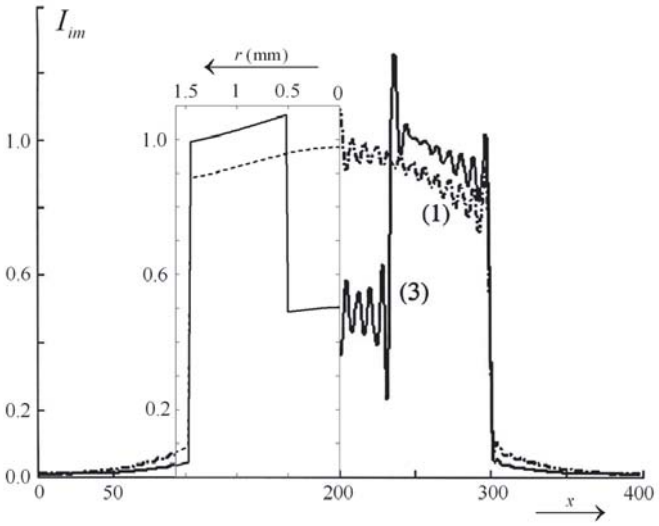

Fig. 3. Profile (1): the same as in Figure 2; profile (3): the same as profile (2) of Figure 2 but for a negative nonlinear phase shift $\varphi_0 = -0.91$ rad.

for $\rho = 0.345$ and $\varphi_0 = -0.91$ rad is also presented in Figure 3. Because the optical transfer function (OTF) of the imaging system is not considered here, the 'ringing effect' is absent [5]. On the contrary, the numerical simulations of reference [1] take into account the OTF which induces signal oscillations at the border of the circular object. Nevertheless, Figures 2 and 3 show that our analytical calculations are in good agreement with the numerical and experimental results shown in reference [1] when one

considers the average of the signal obtained at the right-hand side of these figures. Finally note that in Figure 2 the phase contrast ΔT is given by:

$$\Delta T = \left\langle I^{(\rho)}(r) \right\rangle_{r\in[0,L_P]} - \left\langle I^{(\rho)}(r) \right\rangle_{r\in[L_P,R_a]}, \qquad (13)$$

where the brackets $\langle \dots \rangle$ stand for the average over *area*. This definition, already used in reference [1], corresponds to the difference between the mean values of the diffracted intensity inside the phase plate and the intensity outside.

3.1 First-order approximation ($\varphi_0 < 1$ rad)

In this part, we assume $\varphi_0 < 1$ rad. In this case and if there is no absorption, the phase contrast may be approximated by considering the conservation of the energy in the images given with and without PO (the diffracted energy inside the PO is deflected from outside). A rough but simple calculation given in Appendix A reduces equation (13) to:

$$\Delta T \approx \frac{I^{(\rho)}(0) - 1}{1 - \left(\frac{L_p}{R_a}\right)^2}. \qquad (14)$$

Besides for lossless Kerr medium such as CS_2 where $q_0 \approx 0$, the real functions c_i and s_i can be easily expanded in Taylor series. Thus, we get $s_i = \varphi_0 \sum_{n=0}^{\infty} (-1)^n \varphi_0^{2n} \Upsilon_i^{(2n+1)}$ and $c_i = -\varphi_0^2 \sum_{n=0}^{\infty} (-1)^n \varphi_0^{2n} \Upsilon_i^{(2n+2)}$, with:

$$\begin{cases} \Upsilon_i^{(N)}(r) = 2^{2N} \sum_{q=0}^{N} \frac{1}{q!} \left(2 \sin \frac{\varphi_L}{2}\right)^{2(N-q)} \\ \qquad\qquad \times \sum_{p=N-q}^{2(N-q)} \frac{(-1)^p \mathrm{K}_{p+i}^{(N)}(r)}{(2(N-q)-p)!(p-(N-q))!} \\ \mathrm{K}_p^{(N)}(r) = \rho^p \int_0^{\infty} J_1(v)^{2N+1-p} J_1(v\rho)^p J_0(vr/R_a) v^{-2N} dv. \end{cases} \qquad (15)$$

Taking into account that $\lim_{r\to\infty} \mathrm{K}_p^{(N)}(r) = 0$ and $\lim_{N\to\infty} \mathrm{K}_p^{(N)}(0) = 0$, these expansions show that for a small nonlinear phase shift φ_0, s_i and c_i are roughly proportional to φ_0 and φ_0^2, respectively. At first approximation, $s_i(r) \approx \varphi_0 \Upsilon_i^{(1)}(r)$ and we get:

$$s_i(r) \approx 4\varphi_0 \left(\mathrm{K}_i^{(1)}(r) - 4 \left[\mathrm{K}_{i+1}^{(1)}(r) - \mathrm{K}_{i+2}^{(1)}(r) \right] \sin^2 \frac{\varphi_L}{2} \right). \qquad (16)$$

Moreover considering only the first-order terms in φ_0, equation (11) reduces to:

$$I^{(\rho)}(r) \approx 2s_0(r) \sin\varphi_L \mathrm{circ}(r/L_p) + (1 - 2s_1(r) \sin\varphi_L) \mathrm{circ}(r/R_a). \qquad (17)$$

Using equations (14–17), we thus obtain a linear relation between ΔT and the algebraic value φ_0:

$$\Delta T = \mathfrak{S}\varphi_0 \qquad (18)$$

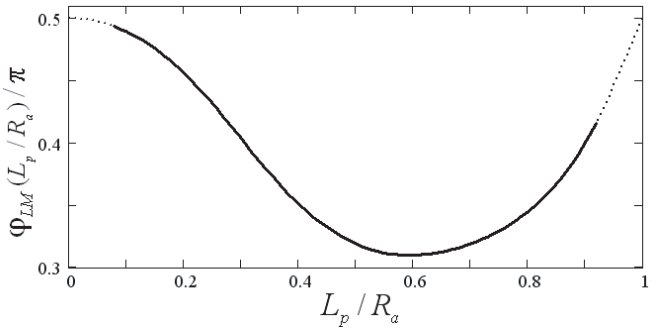

Fig. 4. PO phase shifts $\varphi_{LM}(L_p/R_a)$ giving the best phase contrast in the case of a first-order approximation and for every possible value of the geometric parameter L_p/R_a.

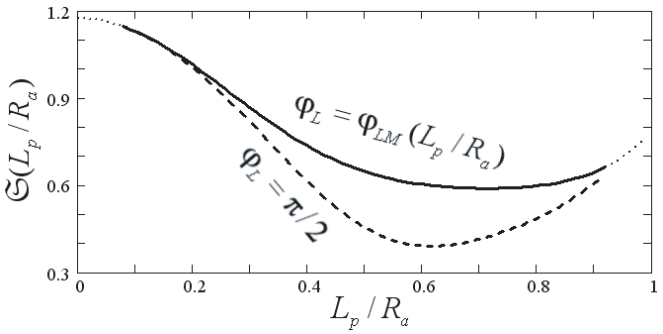

Fig. 5. Sensitivity $\mathfrak{S}$ versus the geometrical factor L_p/R_a calculated using only first-order terms and an approximation of the sensitivity formula for (i) a phase shift of the phase object $\varphi_L = \varphi_{LM}(L_p/R_a)$ providing the best phase contrast (solid line); (ii) $\varphi_L = \pi/2$ (dashed line).

where the sensitivity $\mathfrak{S}$ defined by the ratio of the contrast to the nonlinear phase shift can be approximated by:

$$\mathfrak{S} \approx \frac{16 \sin\varphi_L}{1 - \left(\frac{L_p}{R_a}\right)^2} \left(\Lambda_0 - \Lambda_1 - 4 \left[\Lambda_1 - 2\Lambda_2 + \Lambda_3 \right] \sin^2 \frac{\varphi_L}{2} \right) \qquad (19)$$

with:

$$\Lambda_p = \left(\frac{L_p}{R_a}\right)^p \int_0^{\infty} J_1\left(\frac{vL_p}{R_a}\right)^p \frac{J_1(v)^{3-p}}{v^2} dv. \qquad (20)$$

Finally, equations (18, 19) give simple expressions relating the obtained signal to the induced nonlinear phase shift. This allows an easy experimental determination of the nonlinear index coefficient of the sample under study. The sensitivity reaches a maximum when $\partial\mathfrak{S}/\partial\varphi_L = 0$ for a phase shift φ_{LM} which depends on $\rho = L_p/R_a$. This optimal function $\varphi_{LM}(\rho)$ matches the following relation:

$$2 + \frac{\Lambda_0 - \Lambda_1}{\Lambda_1 - 2\Lambda_2 + \Lambda_3} \approx 8 \sin^2 \frac{\varphi_{LM}}{2} + \frac{2}{\cos\varphi_{LM}}. \qquad (21)$$

In Figure 4, we show the variation of the function $2\varphi_{LM}(\rho)/\pi$ whereas Figure 5 provides the approximated sensitivity as calculated by equation (19) for the two cases: (i) $\varphi_L = \varphi_{LM}(\rho)$; (ii) $\varphi_L = \pi/2$. One can see from Table 1

Table 1. Optimal values of the PO phase shifts and corresponding phase contrasts $\Delta T = \mathfrak{S}\varphi_0$ (for $\varphi_0 = 0.182$ rad) calculated by using a first-order approximation (this work) and those calculated numerically as in reference [1].

$\rho = \frac{L_p}{R_a}$	φ_L/π (this work)	φ_L/π Ref. [1]	$\Delta T_{\max}$ (this work)	$\Delta T_{\max}$ Ref. [1]
0.083	0.49	0.5	0.21	0.21
0.345	0.38	0.39	0.15	0.16
0.690	0.31	0.31	0.11	0.11

that the results obtained in these figures are in good agreement with the numerical results given in reference [1] for a 'small' φ_0 ($\varphi_0 = 0.182$ rad) and the three values of the geometrical parameter $\rho = L_p/R_a$. From Figure 4, it appears that the sensitivity is maximum for $\pi/3 < \varphi_L < \pi/2$ depending on ρ. Moreover, Figure 5 shows that for small values of ρ (i.e., small radii L_p) the signal is higher and the contrast is not significantly affected by the use of a phase object characterized by $\varphi_L = \pi/2$ instead of $\varphi_{LM}(\rho)$, the optimal value. Therefore experimentally, it is preferable to choose $\rho < 0.35$ and $\varphi_L \approx \pi/2$. Note that in Figures 4 and 5, the results obtained in the limit cases for $\rho \to 0$ and $\rho \to 1$ are not shown. We should remember that the OTF of the system was not considered in our analytical calculations. This may introduce errors due to ringing effects at the limit of very small objects or apertures and the analytical results are not valid because the signal obtained from the diffraction at the border is of the same magnitude as that obtained from the nonlinear dephasing.

3.2 Contrast in the general case

In what follows, we consider a high nonlinear phase shift φ_0. The phase contrast ΔT defined by equation (13) can be computed using the analytical equations (9) and (11) or (12). In Figures 6 and 7, we report ΔT versus φ_0 for $|\varphi_0| < 1$ rad and $|\varphi_0| < 25$ rad, respectively. In order to make a comparison with the numerical results of reference [1], we chose for these figures, $\rho = 0.345$ ($L_p = 0.5$ mm and $R_a = 1.45$ mm) and $\varphi_L = \pi/2$.

Figure 6 confirms that ΔT varies, approximately linear with φ_0 as mentioned in reference [1]. The solution is close to the first-order approximation for both $n_2 > 0$ and $n_2 < 0$ (note that higher-order corrections are positive in both cases). Moreover the sensitivity represented by the slope of the curve is in good agreement with the one computed in reference [1] and with the approximation presented in Figure 5 for $\varphi_L = \pi/2$. At least as long as $\varphi_0 < 1$ rad, the $4f$ system using a phase object permits a measurement of the algebraic value of n_2. The analysis becomes more complex when $\varphi_0 > 1$ rad as shown in Figure 7. The contrast ΔT does not vary linearly with φ_0 anymore. Considering the case when $n_2 < 0$, ΔT reaches its negative minimum for $|\varphi_0| = \left|\varphi_0^{\min}\right|$. For larger values of $|\varphi_0|$, it can even be positive. In Figure 7 is shown the evolution of the contrast versus the nonlinear dephasing for the parameters $\rho = 0.345$ and $\varphi_L = \pi/2$ giving

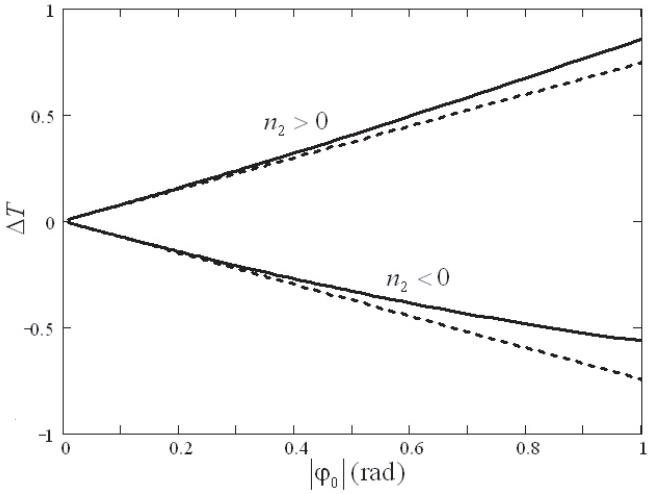

Fig. 6. Phase contrast ΔT versus $|\varphi_0|$ in the case of low nonlinear dephasing ($|\varphi_0| < 1$ rad) for $n_2 > 0$ and $n_2 < 0$ with $\rho = L_p/R_a = 0.345$ and $\varphi_L = \pi/2$. All-order calculations (solid lines) and first-order terms (dashed lines) are shown together.

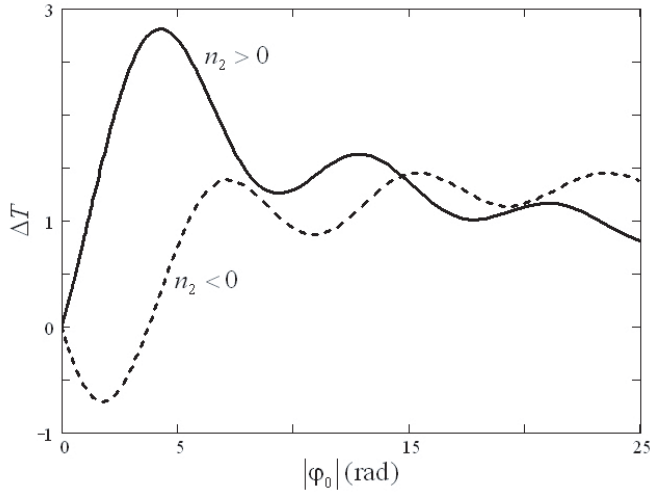

Fig. 7. Phase contrast ΔT versus $|\varphi_0|$ for $|\varphi_0| < 50$ rad, $\rho = 0.345$ and $\varphi_L = \pi/2$. The solid line stands for $n_2 > 0$; the dashed line for $n_2 < 0$.

$\left|\varphi_0^{\min}\right| = 1.8$ rad. One can see in this figure the change of the sign of ΔT at 3.8 rad. In the case when $n_2 > 0$, the function $\Delta T(\varphi_0)$ reaches its maximum for $\varphi_0 = \varphi_0^{\max}$ at few radians (4.3 rad in Fig. 7) and then decreases. For both cases beyond $|\varphi_0| \approx 7$ rad, ΔT oscillates around a saturation value (approximately 1 in Fig. 7). In Figure 8, values of $\left|\varphi_0^{\min}\right|$ and $\varphi_0^{\max}$ are provided as a function of the geometrical factor $\rho = L_p/R_a$ for $\varphi_L = \pi/2$. It is important to note that for ρ higher than 0.7, $\left|\varphi_0^{\min}\right| > \varphi_0^{\max}$ and the saturation value of the contrast becomes negative in both cases when $n_2 < 0$ and $n_2 > 0$. This behavior can be a source of error in the measurement procedure using phase objects if we simply attribute the sign of the contrast to the sign of the nonlinear index.

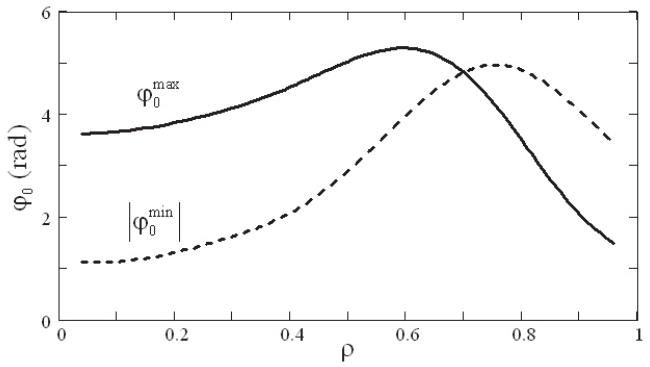

Fig. 8. Values of the first zero of the φ_0-derivative of the phase contrast ΔT, versus ρ for $\varphi_L = \pi/2$: the solid line stands for $\varphi_0^{\max}(n_2 > 0)$; the dashed lines for $\left|\varphi_0^{\min}\right|$ $(n_2 < 0)$.

Mathematically, the evolution of ΔT can be easily understood owing to equations (9) and (11) and to the expansion described by equations (15). More particularly in equation (11), terms which are not in factor of the circ functions are in powers of φ_0 higher than one. They cannot be neglected for high values of $|\varphi_0|$ whereas they correspond to intensities diffracted in the entire image plane and not only in the circular areas limited by the circ functions. Physically, this means that higher the value of $|\varphi_0|$, greater is the part of the energy diffracted outside the image (aperture + PO), thus inducing saturation of the phase contrast. Experimentally, it forbids any measurement of the phase contrast in order to determine n_2 for $|\varphi_0| > \left|\varphi_0^{\min}\right|$ if $n_2 < 0$ and for $\varphi_0 > \varphi_0^{\max}$ if $n_2 > 0$.

4 Conclusion

We have considered a $4f$ system in presence of a phase object in order to measure the nonlinear index coefficient of a nonlinear material placed in the Fourier plane. We obtained the optimized parameters to increase the sensitivity of the measurement. For low intensities, we showed analytically that a linear relation exists between the phase contrast (the signal) and the induced nonlinear phase shift. In this case, a simple first-order relation allows an easy experimental determination of the sensitivity as well as the nonlinear index. We also derived the analytical solution giving the phase contrast for high nonlinear phase shifts. This study shows a limit of using this technique: the saturation of the phase contrast. In particular, it shows what could be a possible source of error in the measurement procedure using phase objects: the sign of the contrast cannot be attributed to the sign of the nonlinear index as simply as it was reported up to now for low nonlinear phase shifts.

Appendix A

For small values of the nonlinear phase shift, the signal $I(r)$ in the image plane can be roughly described in terms of circ functions as:

$$I(r) = I_a \mathrm{circ}(r/R_a) + (I_p - I_a)\mathrm{circ}(r/L_p), \qquad (A.1)$$

where I_a stands for the image of the aperture at the entry of the set-up and I_p is the image of the phase object. Assuming the conservation of the energy with and without the phase object, we get:

$$I_a \pi R_a^2 + (I_p - I_a)\pi L_p^2 = I_0 \pi R_a^2, \qquad (A.2)$$

where I_0 is the signal obtained without the phase object. For a normalized signal ($I_0 = 1$), we obtain:

$$I_p - I_a = \frac{I_p - 1}{1 - \left(\frac{L_p}{R_a}\right)^2}. \qquad (A.3)$$

This equation defines the phase contrast and is similar to equation (14).

References

1. G. Boudebs, S. Cherukulappurath, Phys. Rev. A **69**, 053813 (2004)
2. M. Sheik-Bahae, A.A. Said, T.H. Wei, D. Hagan, E.W. Stryland, IEEE J. Quant. Electron. **26**, 760 (1990)
3. G. Boudebs, C.B. de Araujo, Appl. Phys. Lett. **85**, 3740 (2004)
4. G. Boudebs, S. Cherukulappurath, Opt. Commun. **250**, 416 (2005)
5. J.W. Goodman, *Introduction to Fourier optics*, 2nd edn. (Mc Graw Hill, New-York, 1996)
6. J.A. Hermann, J. Opt. Soc. Am. B **1**, 729 (1984)